Optical and Quantum Electronics (2023) 55:872
https://doi.org/10.1007/s11082-023-05126-8

Thermo-optical properties of gold nanoparticles embedded in the oxygenated and deoxygenated human blood

A. Akouibaa[1] · R. Masrour[2] · M. Benhamou[3] · A. Derouiche[1]

Received: 21 March 2023 / Accepted: 28 June 2023 / Published online: 23 July 2023

Abstract
Gold nanoparticles (GNPs) aided plasmonic photothermal therapy has demonstrated promising results in the treatment of cancer. This treatment requires intravenous or intratumorally injection to insert GNPs into cancer cells and irradiate them with Visible-Near Infrared light that will be converted into heat. In this study, the impact of the shape and morphology of GNPs injected into oxygenated and deoxygenated human blood on their optical properties and their heating capacity have been investigated. Firstly, the numerical finite element method (FEM) is used to determine the effective dielectric constants and absorption spectra of GNPs with various shapes and morphologies such as: solid sphere, hollow sphere, core-SiO_2/gold shell, core-Fe_3O_4/gold shell and gold nanorods (GNRs). It has been shown that the absorption curves of GNPs depend on the oxygenation degree of blood in which they are injected. In particular for oxygen saturated blood the absorption spectrum shows two peaks: the first one which is more pronounced corresponds to the surface plasmons resonance (SPR) of GNPs is located in the visible- near infrared band and the second one which is smaller is located near the UV-blue band. On the other hand, the SPR-peak properties essentially position, and amplitude depend on the shapes of the studied nanoparticles and on the geometrical parameters such as the gold shell thickness for core/shell NPs (Hollow, SiO_2/Au and Fe_3O_4/Au) and aspect ratio (length divided by width) for the GNRs. Second, we studied the thermo-plasmonic properties and local field enhancement at the SPR of spherical GNPs and GNRs injected into oxygen-saturated blood. The obtained results show that the local field enhancement is very important for GNRs compared to the spherical GNPs. The plasmonic heat dissipation of spherical GNPs dispersed in human blood is studied under effect of time and nanoparticle concentration.

Keywords GNPs · Plasmonic · Photothermal therapy · FEM · SiO_2/Au and Fe_3O_4/Au

✉ R. Masrour
rachidmasrour@hotmail.com

[1] LPPSMM, Physics Department, Faculty of Sciences Ben M'sik, Hassan II University Casablanca, P.O. Box 7955, Casablanca, Morocco

[2] Laboratory of Solid Physics, Faculty of Sciences Dhar El Mehraz, Sidi Mohamed Ben Abdellah University, BP 1796, Fez, Morocco

[3] Dynamics of Complex Systems Team, Physics Department, Faculty of Sciences, Moulay Ismail University, P.O. Box 11201, Meknes, Morocco

1 Introduction

Photothermal therapy (PTT) involves using light and a photosensitive "platform" to heat the cells. A local temperature increase of 7 °C is sufficient to destroy the tumor cells that cannot be removed by surgical resection (Kumar et al. 2020; Choi et al. 2012; Hu et al. 2008). Cancer cells are naturally more sensitive to radiation than normal cells. For this reason, a number of protocols, based on hyperthermia, have been developed to destroy tumor cells in an irreversible procedure. Several methods involving laser, microwave, radio frequency and ultrasound have been tested to locally heat a cancerous area and destroy it (Kaur et al. 2016; Wijlemans et al. 2012; Kalber, et al. 2016). PTT using gold nanoparticles (GNPs) represents a promising new therapy for a cancer treatment. It has begun to be used experimentally in patients with specific cancers, but much research is still needed before it can be offered more widely. During the interaction with light, GNPs are well known to be the seat of collective oscillations of conduction electrons. When the frequency of the incident wave corresponds to the natural frequency of these oscillations, a resonance phenomenon occurs, called SPR. The spectral position of this resonance can be easily adjusted from the visible to the infrared band, by modulating the size and the geometry of NPs (Hu et al. 2020). This therapeutic window stems from the fact that the human skin tissues only weakly absorb light with wavelengths between 650 and 900 nm (optical window). Therefore, NIR light can optically penetrate the biological tissues and excite the GNPs embedded inside deeper tumors to generate localized heating.

In addition to their remarkable optical properties GNPs also possess thermal properties of great interest. Due to the strong optical absorption of nanoscale gold, particularly at the plasmon resonance, metal nanoparticles behave as heat nanosources. Indeed, the photon energy absorbed by the particle is converted into thermal energy by Joule effect, which generates a temperature rise ΔT inside the particle. The nanoparticle being hotter than its environment (at the initial temperature T_0), thermal energy is transferred from the particle to the outside (phenomenon thermal diffusion). It then occurs a rise in temperature in the surrounding environment (Baffou 2017; Baffou and Quidant 2013; Jain et al. 2007). It is well known that the plasmonic properties of metal nanoparticles depend strongly on their environment, composition, size and shape. In particular, the SPR-peak of spherical GNPs appears in the vicinity of wavelengths 520–540 nm. To adjust the plasmonic properties, several gold nanostructures that absorb NIR light have been reported, with structures including gold nanorods (Nikoobakht and El-Sayed 2003; Murphy et al. 2005), silica/gold nanoshells (Yu-Chen et al. 2018), Fe_3O_4/gold nanoshells (Wasfi et al. 2019) and hollow GNPs (Loghman Nia and Naderi 2018). For a given plasmonic nanostructure, the SPR profile can be modified by its environment by means of its dielectric constant ε_m (Liao et al. 2018). Then, using the GNPs as therapeutic agents must take into account the dielectric properties of the biological tissues in which they are injected. When a biological tissue is exposed to electromagnetic radiation, interactions occur with the electrical charges of the cells. These interactions can cause biological effects that are not necessarily harmful to health (Sienkiewicz 1994; Ansal et al. 2018). The complexity of these phenomena is due to several factors, in particular the characteristics of the incident wave: its frequency, polarization and intensity and of the tissue encountered (its geometry, its electromagnetic properties: dielectric permittivity and conductivity) (Akouibaa et al. 1244). Several studies are carried out to approximate the frequency variations of dielectric properties of biological media including numerical methods, empirical models and experimental measurements. Including, the Finite-Difference Time-Domain (FDTD) method (Young 1995), Debye and

Cole–Cole models (Lazebnik et al. 2007a, 2007b) and experimental measurements that are listed in the work of Gabriel and Gabriel (Gabriel et al. 1996a, 1996b, 1996c).

The dielectric and optical properties of blood could offer much information that are used in medical diagnosis and therapy. The ability of blood to absorb the different types of spectra is the basis for many therapeutic and diagnostic applications. A number of research studies have been performed on the dielectric properties of blood over a broad frequency range (Alison and Sheppard 1993; Pethig 1984; Liu et al. 2019; Zhernovaya et al. 2011). Measurements of optical properties such as: refractive index, blood in the visible light spectrum and near infrared are the basis of the diagnosis of many blood diseases (Faber et al. 2004; Friebel and Meinke 2006). The principle to using of GNPs in new cancer therapies is to destroy tumors by photothermy that is to locally heating the tumors selectively decorated with gold nanoparticles by illuminating them. In this treatment mode, the first step is to inject the GNPs into the patient's bloodstream by an intravenous injection. GNPs pass unnoticed by the immune defense system, their nanometric size is typically a hundred times smaller than cells, which allows them to circulate freely through the bloodstream and penetrate in the tumor. Many tumors are highly vascularized they have this faculty to build a network blood vessel that allows them to grow. Taking advantage of this pathway, nanoparticles naturally accumulate inside. This increased retention in tumors is promoted by greater permeability of the blood vessels whose structure is altered at the level of tumors. The second step is to illuminate the gold nanoparticles with an electromagnetic wave. At this stage, we must take up a double challenge: The light must penetrate the tissue until the tumor, but healthy tissue must not heat up. The choice of its frequency is therefore essential, it is indeed necessary to illuminate the nanoparticles at their resonant frequency, but it is just as necessary that the tissues without nanoparticles do not absorb this light. In this perspective, the study of the process of the interaction of the Vis–NIR light with the GNPs injected into the blood vessels is essential.

The study of the optical properties of GNPs injected in blood vessels is realized by modeling the system as a nanocomposite inclusions-matrix in which metallic inclusions (GNPs) are dispersed in a dielectric matrix (blood). To quantify the optical properties of nanocomposites requires precise knowledge of the parameters that characterize their dielectric behavior i.e. the effective complex permittivity $\left(\tilde{\varepsilon}_{eff} = \varepsilon' + \varepsilon''\right)$ or the effective complex conductivity $\left(\tilde{\sigma}_{eff} = \sigma' + i\sigma''\right)$. These parameters are given by $\tilde{\sigma} = j\varepsilon_0 2\pi f \tilde{\varepsilon}_{eff}$ where ε_0 is the vacuum permittivity and f is the frequency. The effective permittivity of the nanocomposite is typically calculated using one of the well-known Bruggeman, or Maxwell–Garnett mixing rules (Maxwell–Garnett 1904). It is an accepted fact that the validity of these rules is limited to low volume fractions of inclusions, less than 10–15% and to simple geometric shapes. Moreover, numerical simulation is a powerful tool to solve scientific and engineering problems. It plays an important role in many aspects of fundamental research and engineering applications. FEM is used to study optical and dielectric properties of composite materials at different scales and with complex compositions (Reddy 1989; Akouibaa, et al. 2021).

The dielectric and optical properties of GNPs embedded in human blood were studied by using the FEM. This method allows to calculate the distribution of the electric potential in the nanocomposite when the latter is illuminated by an EM wave. Then the dielectric and optical parameters are calculated, namely: the effective complex permittivity and the absorption cross section. First, we present a comparative study of the plasmonic properties of GNPs injected into the blood of different shapes: spherical gold nanoparticle (SGNP), hollow HGNP, core-SiO_2/Shell-Gold (SiO_2/Au), core-Fe_3O_4/Shell-Gold (Fe_3O_4/Au) and gold nanorods (GNRs). For a core/shell structures (HGNP, SiO_2/Au and Fe_3O_4/Au) we

study the effect of the gold shell thickness on the shifting of the plasmonic band in the Vis–NIR spectrum, and the same for the GNRs the effect of the aspect ratio (the length (L) divided by the width (W)) is studied. Since oxygen is an essential component of the blood it plays a key role in their optical properties, we also present a comparative study of the optical properties of these GNPs in oxygenated and deoxygenated blood. In the second step we present a thermoplasmonic study of SGNPs and GNRs, for this we are studying the local electric field exaltation and the generated plasmonic heat at the nanometric scale. Finally, the study is extended to determine the heating capacity throughout the medium as function of the concentration of the GNPs (in ppm units).

2 Physical model and numerical method

To evaluate the optical properties of GNPs injected into human blood, we model the system as a two or three-phase heterostructure (matrix-inclusions) in which the (GNPs) are periodically dispersed in a blood medium. The numerical FEM that we present here allows to calculate the effective optical parameters of nanocomposites from the microscopic properties of their constituents. In order to consider the uniform field in the whole particle, the modelling of the study is performed within the framework of the quasi-static approximation in which the size of the inclusions is smaller than the wavelength. The implementation of this method is carried out following the steps: (i) Determination of the computational elementary domain that contains the inclusion with definition of the geometry, the volume fraction and the relative permittivity of each component. (ii) Meshing the entire domain in tetrahedral finite elements. (iii) Calculation of the spatial distribution of local potential in the considered domain with zero charge and current density. This distribution is obtained by solving the Laplace's equation:

$$\vec{\nabla}\left(\varepsilon_0 \varepsilon\left(\vec{r}\right)\vec{\nabla} V\left(\vec{r}\right)\right) = 0 \tag{1}$$

$\varepsilon\left(\vec{r}\right)$ is the local relative permittivity, $V\left(\vec{r}\right)$ is the local potential and $\varepsilon_0 = 8.85.10^{-12}\mathrm{F/m}$ is the permittivity of the vacuum.

The basic scheme of the FEM is shown in Fig. 1 wherein we consider the calculation domain is incorporated into parallel plate capacitor, with conducting plates of area S and separation distance h which is filled with the composite medium to be studied. A

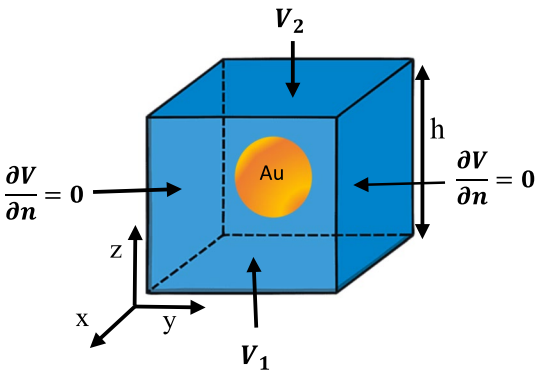

Fig. 1 Elementary calculation cell with periodic boundary conditions

constant potential difference $(V_2 - V_1)$ is kept between the capacitor plates. At each element resulting from the subdivision, the function modeling the potential and its normal derivative are defined by a polynomial interpolation (Sareni et al. 1996; Myroshnychenko and Brosseau 2005a, b; El-Kady et al. 2013).

$$V = \sum_{i=1}^{n} \lambda_i V_i \tag{2}$$

$$\frac{\partial V}{\partial n} = \sum_{i=1}^{n} \lambda_i \left(\frac{\partial V_i}{\partial n} \right) \tag{3}$$

where λ_i are the interpolation functions, n is the number of interpolation nodes and V_i the nodal values. The basic principle is to find the distribution of nodal values λ_i that verify the partial differential equations and satisfy the boundary conditions.

The electrostatic energy δW_e^k, and losses δP_e^k can be calculated from the values of the derivatives potential at the mesh nodes over the entire composite domain using the equations:

$$\delta W_e^k = \frac{\varepsilon_0}{2} \iiint_{V_k} \varepsilon_k'(x,y,z) \left[\left(\frac{\partial V}{\partial x} \right)^2 + \left(\frac{\partial V}{\partial y} \right)^2 + \left(\frac{\partial V}{\partial z} \right)^2 \right] dV_k, \tag{4}$$

$$\delta P_e^k = \frac{\varepsilon_0}{2} \iiint_{V_k} \omega \varepsilon_k''(x,y,z) \left[\left(\frac{\partial V}{\partial x} \right)^2 + \left(\frac{\partial V}{\partial y} \right)^2 + \left(\frac{\partial V}{\partial z} \right)^2 \right] dV_k. \tag{5}$$

where ε_k and V_k represent the permittivity and the volume of the kth tetrahedron element, respectively. Thus, the total energy W_e and losses P_e in the entire composite can be written by summation over the n_k elements. The effective permittivity $\varepsilon_{eff} = \varepsilon'_{eff} + i\varepsilon''_{eff}$ in the direction of the applied electric field is obtained by the continuity condition of the normal component of the electric displacement vector via:

$$\iiint_v \varepsilon_z \left(\frac{\partial V}{\partial n} \right)_z = \varepsilon_{eff} \frac{V_2 - V_1}{h} S \tag{6}$$

This relation allow to determine the real ε'_{eff} and imaginary ε''_{eff} parts of the effective permittivity allowing the calculation of the refractive index n_{eff} and the extinction coefficient κ_{eff} which are given by: $\varepsilon'_{eff} = n^2_{eff} - \kappa^2_{eff}$ and $\varepsilon''_{eff} = 2n_{eff}\kappa_{eff}$. (Liu et al. 2014):

In the case where the dimensions of inclusions are very small compared to the wavelength, the light scattering can be ignored, then extinction cross-section σ_{ext} is dominated by the absorption $\left(\sigma_{ext} \approx \sigma_{asb}\right)$. σ_{asb} is obtained by Crut et al. (2014):

$$\sigma_{abs} = \frac{V_p}{f} \frac{k}{n_{eff}} \varepsilon''_{eff} \tag{7}$$

With, V_p and f are the common volume and the volume fraction of the NPs, respectively. k is the wave-vector amplitude of the electromagnetic wave.

3 Results and discussion

3.1 Dielectric permittivity of blood

We recall that the studied system in the present work is a nanocomposite consisting of nanometric inclusions (GNPs) which are periodically dispersed in a dielectric matrix (blood). For this system, we will use the FEM to determine the optical properties and heat generation at SPR in the UV–Vis-NIR spectral band. To respect the quasi-static approximation i.e. the material size must be less than the incident wavelength the macroscopic system is reduced to an elementary cell of nanometric size. The important optical properties (absorption and scattering) of a material are related to the complex refractive index. Under the action of an electromagnetic field a medium becomes polarized, this polarization is result to the movement of the electronic cloud in relation to the nuclei, leading to a shift between the barycenters of negative and positive charges. This polarization will induce a variation of the complex refractive index $\tilde{n}(\omega)$ which is related to the dielectric constant by: $\tilde{n}^2(\omega) = \tilde{\varepsilon}(\omega)$.

The determination of the optical behavior of human blood is a complex task: light is absorbed and scattered by the different blood components (Tuchin 2016; Friebel and Meinke 2005; Ghosh 2006).

In this work we used the data of the optical properties of blood provided by N. Bosschaart et al. (Bosschaart et al. 2014) to calculate their complex refractive index and dielectric permittivity. These authors performed a critical examination and selection of available optical property spectra of blood in the literature, from which they compiled mean spectra for absorption coefficient (μ_a), scattering coefficient (μ_s), and the diffusion anisotopy (g). The imaginary part $\kappa(\omega)$ of the complex refractive index $\tilde{n}(\omega) = n(\omega) + i\kappa(\omega)$ is related to the absorption coefficient μ_a through:

$$\kappa(\omega) = \frac{c\mu_a(\omega)}{2\omega} \tag{8}$$

where c is the speed of light and ω is the angular frequency of the light. This relation is expressed by the Kramers–Kronig (KK) integral dispersion equations (Faber et al. 2004; Lucarni et al. 2005):

$$n(\omega) = n(\omega_0) + \frac{2}{\pi}(\omega^2 - \omega_0^2)P\int_0^\infty \frac{\omega'\kappa(\omega')}{(\omega^2 + \omega')(\omega_0^2 - \omega')}d\omega' \tag{9}$$

where $n(\omega_0)$ is the refractive index at some reference frequency ω_0, providing scaling of the calculated spectra. P denotes the Cauchy principal value of the integral.

The real ε' and imaginary ε'' parts of the complex permittivity of blood are given from the complex refractive index by $\varepsilon' = n^2 - \kappa^2$ and $\varepsilon'' = 2n\kappa$, the real refractive index n describes energy storage and the imaginary refractive index κ describes energy dissipation and specifies the extinction coefficient (Jacques 2013). Figure 2a, b shows the spectra of the real and imaginary parts of the dielectric permittivity of oxygenated and deoxygenated blood with a hematocrit of 45% (red blood cell concentration) (Meinke et al. 2007; Steinke and Shepherd 1988; Faber and Leeuwen 2009).

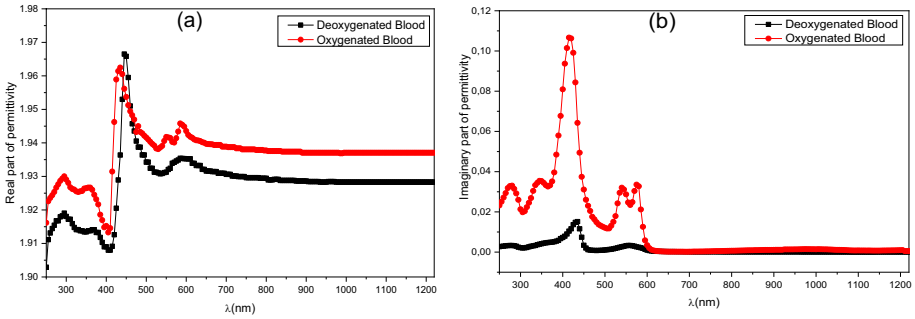

Fig. 2 The plots of **a** real and **b** imaginary parts of complex permittivity of oxygenated and deoxygenated blood against the wavelength

3.2 Shape effect on the optical properties of GNPs embedded in blood

In this section we present a comparative study of the dielectric and optical properties of GNPs with different shapes injected into oxygenated and deoxygenated human blood. For this we perform a series of simulation using FEM, we consider a GNPs with the following shapes: spherical (SGNP), hollow sphere (HGNP), core-SiO_2/Shell-Au (SiO_2/Au), core-Fe_3O_4/Shell-Au (Fe_3O_4/Au) and nanorod (GNR), these nanoparticles are embedded separately into oxygenated and deoxygenated human blood. The chosen geometric parameters for this simulation are: (i) for SGNPs the radius is $r = 20$ nm, (ii) for the other spherical core/shell shapes the total radius $r_t = 20$ nm $\left(r_t = r_c + e\right)$ with $r_c = 15$ nm is the core radius (area, SiO_2 and Fe_3O_4 respectively for the HGNPs, SiO_2/Au and Fe_3O_4/Au shapes) and $e = 5$ nm is the gold shell thickness, (iii) for the GNRs the length ($L = 72.68$ nm) and the width ($W = 24.22$ nm), these parameters are chosen such that all nanoparticles have the same volume. The volume fraction of the nanoparticles is chosen $f = 0.05$ which is equal in the elementary simulation cell to the volume of the particle divided by the total volume of the cell.

To determine the complex permittivity, we have used the Drude model (Vial and Laroche 2008). Figures 3a, b and 4a, b report the evolution of the real and imaginary parts of

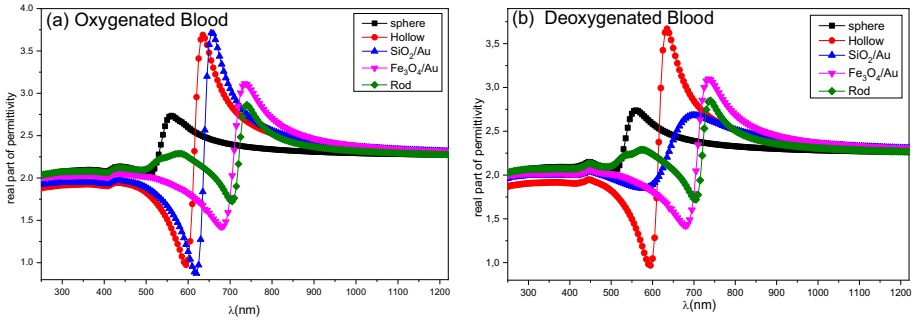

Fig. 3 The plots of $\varepsilon'_{eff}(\lambda)$ against the wavelength, for the following nanoparticles: SGNPs, HGNPs, SiO_2/Au, Fe_3O_4/Au and GNRs that have the same volume and embedded in the **a** oxygenated and **b** deoxygenated blood

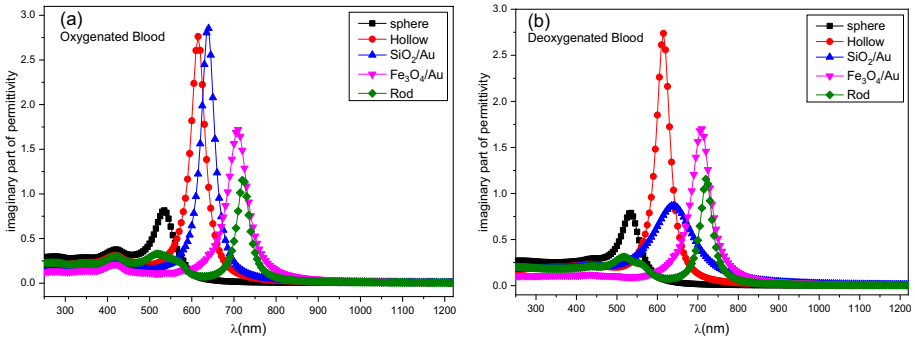

Fig. 4 The plots of $\varepsilon''_{eff}(\lambda)$ against the wavelength, for the following nanoparticles: SGNPs, HGNPs, SiO_2/Au, Fe_3O_4/Au and GNRs that have the same volume and embedded in the **a** oxygenated and **b** deoxygenated blood

the dielectric permittivity as a function of the wavelength, of SGNPs, HGNPs, SiO_2/Au, Fe_3O_4/Au and GNRs nanoparticles injected into oxygen-saturated human blood (Figs. 3a, 4a) and in deoxygenated blood (Figs. 3b, 4b). For the HGNPs the permittivity of the core is chosen equal to that of the vacuum ε_0 and for the gold nanoshells SiO_2/Au and Fe_3O_4/Au the permittivity of the silica and iron oxide (magnetite) cores are calculated from the refractive index available in the references respectively (Malitson 1965; Tan 1998) and (Querry 1985). These curves show that the real ε'_{eff} and imaginary ε''_{eff} parts of the effective permittivity widely vary in vicinity of a wavelength $\lambda = \lambda_{\max}$. This domain of strong variation of ε'_{eff} and ε''_{eff} correspond to a high dependence of the propagation speed of electromagnetic wave on the pulsation, the medium is therefore dispersive. Figures 3a, 4a show that in the vicinity of $\lambda_{\max}$, ε'_{eff} varies between two asymptotic values $\varepsilon'_{\min}$ and $\varepsilon'_{\max}$, it is remarkable that the difference $\Delta\varepsilon'_{eff} = \varepsilon'_{\max} - \varepsilon'_{\min}$ is very large in the case of HGNPs and SiO_2/Au nanoparticles compared to other structures. For SGNPs, HGNPs, Fe_3O_4/Au and GNRs nanoparticles, $\Delta\varepsilon'_{eff}$ is identical for oxygenated and deoxygenated blood while for SiO_2/Au nanoparticles this difference is all the greater in the case of oxygenated blood in comparison with deoxygenated blood.

Figures 3b and 4b show that the imaginary part ε''_{eff} takes a maximum for $\lambda = \lambda_{\max}$ which corresponds to a strong absorption of the incident wave which allows estimating the SPR-peak position. It is clearly shown that the peak amplitude presented in the spectrum of ε''_{eff} is more pronounced in the case of HGNPs and SiO_2/Au nanoparticles compared to other structures. For SiO_2/Au nanoparticles, the amplitude of this peak is greater in the oxygenated blood compared to deoxygenated blood, while for other structures there is no difference. Figure 5a, b show the evolution of the absorption cross section calculated from the relation (7) of the nanoparticles: SGNPs, HGNPs, SiO_2/Au, Fe_3O_4/Au and GNRs, embedded in the oxygenated and deoxygenated blood. These curves show a strong dependence of the GNPs absorption spectrum on their morphologies and on the oxygen saturation of the blood in which they are inserted. The absorption spectra of all these nanoparticles show the presence of a small peak in the vicinity of the blue at $\lambda = 415$ nm in the case of the oxygenated blood, this peak does not exist for the deoxygenated blood, which is explained by the strong absorption of oxygen in this band. In addition, for both blood the absorption spectra show a main peak more amplified localized in the vicinity of the

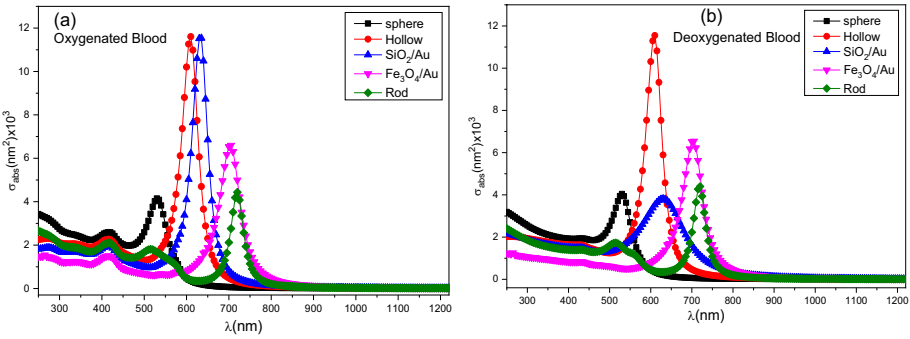

Fig. 5 The plots of the absorption cross section against the wavelength, for the following nanoparticles: SGNPs, HGNPs, SiO_2/Au, Fe_3O_4/Au and GNRs that have the same volume and embedded in the **a** oxygenated and **b** deoxygenated blood

characteristic wavelength $\lambda_{\max}$ corresponds to the SPR. This peak has the same characteristics when the nanoparticles are found in oxygenated or deoxygenated blood with an exception for SiO_2/Au nanoparticles where the amplitude of the absorption peak is very important in the case of oxygenated blood compared to deoxygenated blood. The wavelengths corresponding to the SPR indicated by these curves for the nanoparticles SGNPs, HGNPs, SiO_2/Au and Fe_3O_4/Au are respectively $\lambda_{\max} = 530$ nm, $\lambda_{\max} = 610$ nm, $\lambda_{\max} = 635$ nm and $\lambda_{\max} = 705$ nm annotate that these nanoparticles having the same volume V_{sphere}. In the case of the GNRs the absorption spectrum shows two SPR-peaks, the first is localized in the visible at $\lambda_{\max} = 530$ nm which corresponds to the excitation of the transverse mode plasmons i.e. the conduction electrons collectively oscillate in the transverse direction of the rod, the second peak more pronounced is located in the NIR at $\lambda_{\max} = 720$ nm which corresponds to the excitation of the longitudinal mode where the electrons oscillate along the length of the rod, here the GNRs are chosen of the same volume as the previous spherical structures $V_{sphere} = V_{rod}$.

It is known that the SPR-peak of the SGNPs is located in the visible band between $\lambda_{\max} = 520$ nm and $\lambda_{\max} = 575$ nm when their sizes vary between 10 and 100 nm (Huang and El-Sayed 2010). One of the major problems that arises when using GNPs in therapy is the low penetration of visible light who must excite the plasmonic nanoparticles located in deep tissue. To overcome this problem, it is essential to use the GNPs with other shapes and morphology such as: HGNPs, SiO_2/Au, Fe_3O_4/Au and GNRs in order to obtain the SPR in the near infrared region. In the following we will examine the effect of the gold shell thickness on the plasmonic properties of the core/shell nanostructures (HGNPs, SiO_2/Au and Fe_3O_4/Au) injected into oxygenated human blood. We will introduce a geometric parameter denoted η which is equal to the gold shell thickness e divided by the total radius of the particle r_t, $\eta = \frac{e}{r_t}$ such as $r_t = r_c + e$, with r_c is the core radius. Similarly, we will examine the effect of the aspect ratio denoted ρ on the plasmonic properties of GNRs. Figure 6a–c show the evolution of the absorption cross section of core/shell nanoparticles, HGNPs, SiO_2/Au and Fe_3O_4/Au embedded in oxygenated blood for different values of η. These curves are obtained with the total radius of particles is fixed at $r_t = 20$ nm and the gold shell thickness varies between $e = 2$ nm and $e = 20$ nm i.e. the ratio η varies between 0.1 and 1. These curves show that for these three structures when $\eta = 1\ (e = r_t)$, the SPR-peak is located at $\lambda_{\max} = 530$ nm which

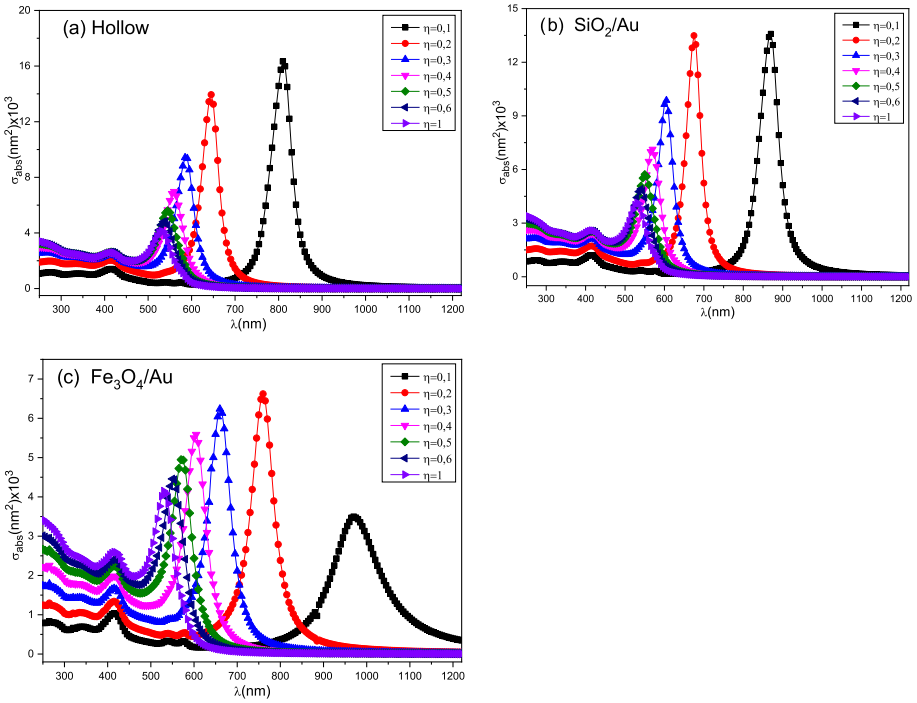

Fig. 6 The plots of the absorption cross section against the wavelength of the core/shell nanoparticles: HGNPs, SiO_2/Au and Fe_3O_4/Au embedded in the oxygenated blood for different value of η

corresponds to the plasmonic resonance of a simple nanosphere. When the gold shell thickness decreases the SPR-peak position shifts towards the NIR. For $\eta = 0.1$ i.e. $e = 2$ nm the SPR-peak occurs for the wavelengths: $\lambda_{max} = 810$ nm, $\lambda_{max} = 870$ nm and $\lambda_{max} = 970$ nm respectively for the HGNPs, SiO_2/Au and Fe_3O_4/Au nanoparticles.

These curves also show that: for the HGNPs the amplitude of the SPR-peak increases considerably when η decreases from 1 to 0.1, for the SiO_2/Au nanoparticles the peak amplitude increases between 1 and 0.6 and remains stable between 0.6 and 0.1 and for Fe_3O_4/Au nanoparticles the amplitude increases between 1 and 0.2 and decreases between 0.2 and 0.1. In addition, all these spectra show the presence of a small peak in the blue $\lambda = 415$ nm which is independent of the particles shape which corresponds to the absorption of oxygenated blood. Figure 7 shows the plot of the absorption spectra of the GNRs for several values of the aspect ratio, these curves are obtained by varying the length L and the width W of the rod while keeping the fixed volume which is equal to the volume of a spherical nanoparticle with radius $r = 20$ nm. These curves show the presence of three absorption peaks: the first in the blue ($\lambda = 415$ nm) corresponds to the absorption of oxygenated blood, the second peak located in the visible ($\lambda = 530$ nm) corresponds to the excitation of the transverse mode of the nanorod and the third main peak located in the NIR which corresponds to the excitation of the longitudinal mode. When the aspect ratio increases: the first two peaks remain in the same positions and their amplitudes decrease slightly, on the other hand the peak of the longitudinal mode

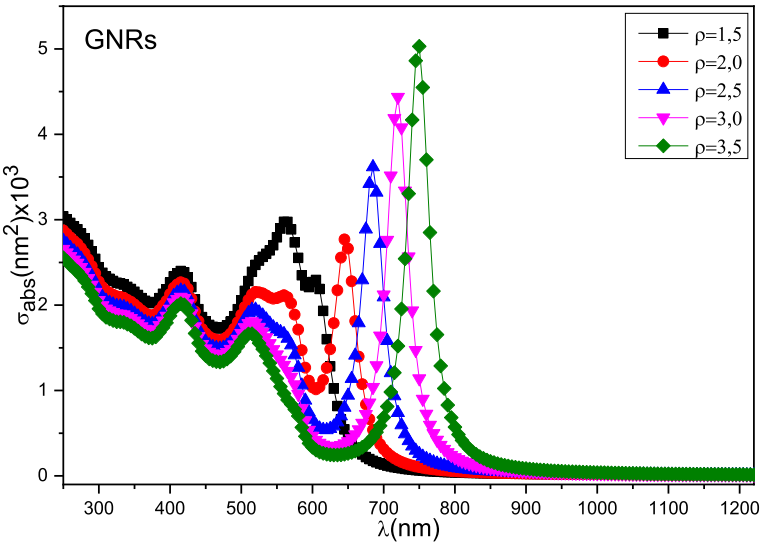

Fig. 7 The plots of the absorption cross section against the wavelength of GNRs embedded in the oxygenated blood for different value of the aspect ratio ρ

shifts towards the NIR and their amplitude increases considerably. It is also remarkable that for low aspect ratios i.e. the length and width become closer, the peak of the longitudinal mode begins to disappear and the absorption spectrum reduces to a single peak it is identical to the spectrum of an isotropic nanoparticles.

The optical properties of GNPs, dictated by their free conduction electrons, give them great possibilities to interact with an electromagnetic field. Submitted to an incident radiation, the electrons of a metallic nanoparticles, naturally little linked to the atom nuclei oscillate collectively creating a wave called plasmon. It is only the application of an incident radiation energy strictly equal to that of the localized surface plasmon that can give rise to the SPR condition. This resonance has the particularity of locally amplifying the incident electromagnetic field, known by the local field exaltation. Under an excitation by an incident field E_i was created a local field in the vicinity of the particle which can be written as follows: $E_{loc} = E_0 + E_r$, with E_r is the depolarization field expressed in the case of the spherical particle as follows: $E_r = -\frac{P}{3\varepsilon_0 \epsilon}$, where P is the polarization of the particle (Sihvola and Kong 1988). The enhancement factor of the local field is defined by: $g = \frac{E_{loc}}{E_0}$ (Smith and Silva 2009). Figure 8a, b shows the evolution of the norm of the exalted local field in the vicinity of SGNPs and GNRs embedded in oxygenated human blood in the UV–Vis-NIR band, these two particles are chosen with the same volume $V_{sphere} = V_{rod}$. These curves are obtained from the potential distribution calculated by the FEM for different values of the incident field norm E_0. These curves show a strong amplification of the local field in the SPR band, the exaltation factor of the field is $g = 2.6$ for the SGNPs and $g = 4.1$ for the GNRs which is independent of the norm of the incident field. We see that the exaltation of the field by plasmonic resonance is approximately twice as important in GNRs compared to SGNPs with the same volume fraction.

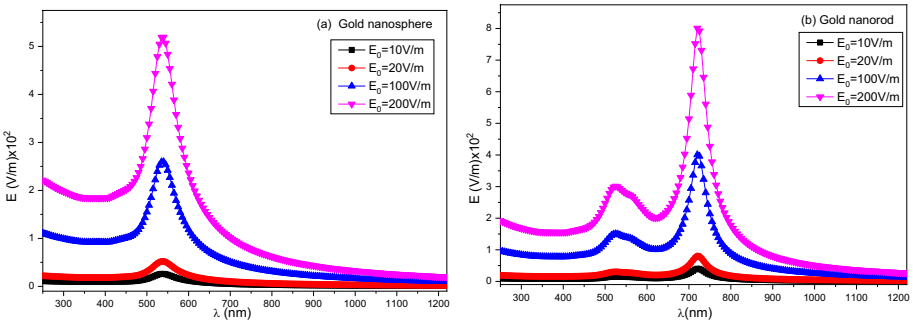

Fig. 8 Electric field exaltation in the vicinity of the gold nanoparticles **a** SGNPs and **b** GNRs embedded in oxygenated blood in the plasmonic band for various values of the incident field norm

The thermo-optical response of GNPs is strongly affected by the local electromagnetic field enhancement at the SPR (Rashidi-Huyeh and Palpant 2006). The increased SPR induced heating rates of GNPs can be explained by the charge movement through resonant nanoparticles and by the higher resistivity of small metal nanostructures compared to bulk metals (Wiley et al. 2006).

The amount of Joule heat generated by each GNPs under SPR oscillations can be directly estimated by approximating GNPs as conductors of constant cross section (Link et al. 1999):

$$P = RI^2 = \sigma(\omega)\left[S \cdot d \cdot E^2\right] \tag{10}$$

where P is the power dissipated as heat, I is the current, and R is the resistance. $\sigma(\omega)$ is the Drude model conductivity of GNP, E is the magnitude of the electric field, S is the cross-sectional area of the gold nanoparticle, and d is its diameter. Assuming efficient heat transfer from n nanoparticles to the surrounding medium here the blood, the heating rate induced by volumetric (dT/dt) of GNP is shown in the following relation:

$$\frac{dT}{dt} = \left[\frac{\sigma(\omega)\left(S \cdot d \cdot |E|^2\right)}{VC_{blood}}\right] \cdot n \tag{11}$$

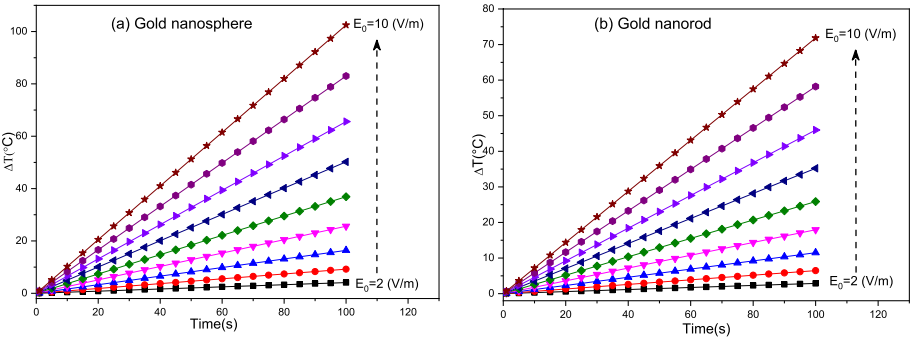

Fig. 9 Variation of the local temperature at plasmonic resonance of **a** SGNPs and **b** GNRs nanoparticles embedded in human blood time-dependent for the values of the incident field varying between 2 V/m and 10 V/m

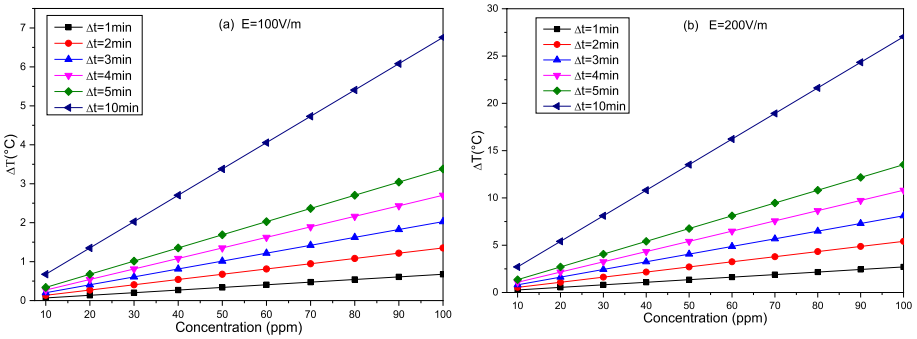

Fig. 10 Temperature increase in the medium blood produced by the SGNPs at plasmonic resonance time-dependent for two various values of the incident field **a** $E_0 = 100$ V/m and **b** $E_0 = 200$ V/m

where V is the volume of the elementary cell containing the particle and the medium and C_{blood} the heat capacity of the blood $C_{blood} = 3.44\ \mathrm{Jml}^{-1}\ ^{\circ}\mathrm{C}^{-1}$. Figure 9a, b show the plots of the local temperature changes ΔT at SPR as a function of time for selected incident field norms of two gold nanoparticles that have the same volume, SGNPs, $r = 20$ nm (Fig. 9a) and GNRs, $L = 72.68$ nm and $W = 24.22$ nm (Fig. 9b). These curves show that the converted heat by the SGNPs and GNRs particles increases linearly with time for a fixed value of E_0, the slope of the ΔT function increases when the norm of the incident field increases. It is clearly shown that the plasmonic heat produced by a gold nanosphere is greater compared to that produced by of gold nanorod, which is explained by the greater resistivity in a sphere compared to the rod. Indeed, in a rod the oscillation of free electrons is carried out according to the longitudinal dimension L which is greater than the sphere diameter d according to which the charges oscillate in the latter. In particular for the norm of the incident field E_0 : $2\ \mathrm{V/m}, 6\ \mathrm{V/m}$ and $10\ \mathrm{V/m}$ and during the time $\Delta t = 100$ s the increase of the plasmonic temperature can reach respectively 4.1 °C, 36.9 °C and 102 °C for a SGNP and 2.9 °C, 25.9 °C and 72 °C for a GNR. Table 1 shows the temperature variations observed near a spherical gold nanoparticle (SGNP) and a gold nanorod (GNR) during plasmon resonance, as a function of different light exposure times and electromagnetic field intensity.

Consider that the GNPs are distributed periodically in the blood tissue and the dissipation of plasmonic heat is uniform throughout the medium. Indeed, uniform distribution of GNPs in human blood means dispersing them homogeneously throughout the medium, avoiding preferential agglomeration in one region over another. This approach assumes that the composite medium GNPs-blood is made up of identical units that reproduce throughout the medium. All nanoparticles behave in the same way and produce the same thermo-plasmonic effect in their blood environment, meaning that plasmonic heat dissipation is uniform throughout the medium. In practical terms, to achieve a uniform distribution of GNPs in the bloodstream, it is necessary to follow the following procedure: once GNPs have been synthesized, their surface must be functionalized to improve their stability and prevent aggregation. This is achieved by coating the nanoparticles with molecules such as citrate, polyethylene glycol (PEG) or other surface ligands that provide steric stabilization (Amina and Guo 2020). Figure 10a, b show the temperature changes throughout the blood medium due to plasmon heat dissipation by an SGNP ($r = 20$ nm) as a function of the particle concentration in ppm units

Table 1 Temperature values in the vicinity of a SGNP and GNP during SPR for different light exposure times and electromagnetic field intensity values

	ΔT(°C) Sphere gold nanoparticles					ΔT(°C) Gold nanorod				
Times $\Delta t(s)$	$E_0 = 2$ V/m	$E_0 = 4$ V/m	$E_0 = 6$ V/m	$E_0 = 8$ V/m	$E_0 = 10$ V/m	$E_0 = 2$ V/m	$E_0 = 4$ V/m	$E_0 = 6$ V/m	$E_0 = 8$ V/m	$E_0 = 10$ V/m
20 s	0,82	3,28	7,38	13,12	20,49	0,57	2,30	5,18	9,20	14,37
40 s	1,64	6,56	14,75	26,23	40,99	1,15	4,60	10,35	18,39	28,74
60 s	2,46	9,84	22,13	39,35	61,48	1,72	6,90	15,52	27,59	43,11
80 s	3,28	13,12	29,51	52,47	81,97	2,30	9,20	20,70	36,78	57,47
100 s	4,10	16,40	36,89	65,58	102,47	2,87	11,50	25,86	45,98	71,84

Table 2 Temperature variations induced by SGNPs dispersed in human blood for different nanoparticle concentrations in (ppm) and different light exposure times

	ΔT(°C) $E_0 = 100$ V/m					ΔT(°C) $E_0 = 200$ V/m				
Times Δt	C (ppm) 20	C (ppm) 40	C (ppm) 60	C (ppm) 80	C (ppm) 100	C (ppm) 20	C (ppm) 40	C (ppm) 60	C (ppm) 80	C (ppm) 100
1 min	0.134	0.27	0.41	0.54	0.68	0.54	1.08	1.62	2.16	2.70
2 min	0.27	0.54	0.81	1.08	1.35	1.08	2.16	3.24	4.33	5.40
3 min	0.41	0.81	1.22	1.62	2.03	1.62	3.24	4.87	6.49	8.11
4 min	0.54	1.08	1.62	2.16	2.70	2.16	4.33	6.49	8.65	10.81
5 min	0.68	1.35	2.03	2.70	3.38	2.70	5.41	8.11	10.81	13.52
10 min	1.35	2.70	4.06	5.41	6.76	5.41	10.81	16.22	21.62	27.04

for several values of the radiative exposure time. These curves show that the dissipated plasmon heat in the blood increases linearly with the concentration of the particles. For the selected values of the incident field $E_0 = 100$ V/m and $E_0 = 200$ V/m, the temperature of the GNPs-blood nanocomposite increases respectively by 7 °C and 27.5 °C for a time 10 min. The plasmonic thermal power dissipated per gram of gold is the ratio of the thermal energy delivered in solution to the total mass of the gold in suspension. Therefore, the thermal power dissipation of the gold nanosphere $r = 20$ nm under the SPR conditions was remarkable about: 3.66 W/g, 366 W/g and 977 W/g respectively for incident field norms 10 V/m, 100 V/m and 200 V/m. Table 2 shows the temperature variations induced by SGNPs dispersed in a blood medium during plasmon resonance, as a function of different nanoparticle concentrations in parts per million (ppm) and different resonant light exposure times. These results offer the possibility to estimate the conditions of use the GNPs injected into oxygenated and deoxygenated human blood in therapy and diagnostics. Particularly the nanoparticles size for a given shape and their concentrations, the amplitude of the incident field and the irradiation time. This study can contribute to many searches on the GNPs, which is a very promising tool for this. Concern the improvement of the treatment conditions to decrease the radiation doses received by the patient, and to increase the effectiveness of the treatment by a more precise localization of the irradiation zone.

4 Conclusion

To conclude, in the first part of this paper we performed a numerical study using the FEM of the optical properties of GNPS with different morphology, SGNPs, HGNPs, SiO_2/Au, Fe_3O_4/Au and GNRs injected into oxygenated and deoxygenated human blood. The study is carried out by modeling this system by a multiphasic inclusion-matrix nanocomposite in which the GNPs are periodically dispersed in the blood. In the framework of the quasi-static limit the real system of infinite dimensions is reduced in to elementary cell with periodic boundary conditions. The several phases of the nanocomposite are characterized by their dielectric permittivity which depend on the frequency of the incident electromagnetic wave. In this work we modeled the permittivity of gold by the two-CPDM, the complex permittivity of oxygenated and deoxygenated blood is determined depending on the frequency from the absorption coefficient available in the literature, we also calculated the permittivity of SiO_2 and Fe_3O_4 from their refractive indices in the UV–Vis-NIR band. The FEM allows to calculate the effective permittivity $\tilde{\varepsilon}_{eff} = \varepsilon'_{eff} + i\varepsilon''_{eff}$ from the resolution of the Laplace equation in the considered domain thus the absorption cross section σ_{abs} is obtained and the plasmonic properties are deduced. The obtained results show a strong dependence of the spectra of the ε'_{eff}, ε''_{eff} and σ_{abs} of GNPs on their shapes and on the oxygen saturation of the blood where they are injected. In the vicinity of the wavelength $\lambda_{\max}$ corresponding to the SPR of the gold nanostructures, the real parts ε'_{eff} undergo a very strong change between two extreme values at the same time the imaginary part takes a maximum value. These changes are very significant in the gold nanoshells, HGNPs and SiO_2/Au compared to other structures SGNPs, Fe_3O_4/Au and GNRs. For all these particles, the absorption spectrum shows the appearance of a secondary peak near the blue at $\lambda = 415$ nm when these particles are injected into oxygenated human blood, this peak which is due to the oxygen absorption in this band disappears in the case of deoxygenated blood. For all these nanoparticles which have the same volume the main peak which

appears with the same characteristics in both cases oxygenated and deoxygenated blood, This SPR-peak is shifted differently depending on the shape towards the near infrared in the following order: GNRs, Fe_3O_4/Au, SiO_2/Au, HGNPs and SGNPs. The peculiarity for GNRs is that their spectra show two plasmonic absorption peaks, the main peak is due to the resonance of the longitudinal mode which is localized in the NIR band and the second less intense located in the visible is due to the resonance of the transverse mode. The study of the composition effect of the core/shell nanoparticles, HGNPs, SiO_2/Au and Fe_3O_4/Au shows that when the gold shell thickness decreases the SPR-peak position shifts towards the NIR. This shift is more significant for these nanoshells in the following order: Fe_3O_4/Au, SiO_2/Au and HGNPs. For GNRs our study shows that when the aspect ratio increases, the SPR-peak shifts towards the NIR. This study makes it possible to estimate the SPR wavelength of these nanoparticles when they are injected into oxygenated and deoxygenated human blood. Effectively the SPR-peak position and the absorption amplitude can be adjusted by modifying the thickness of the gold shell in the HGNPs, SiO_2/Au and Fe_3O_4/Au nano-shells and by modifying the longitudinal and transverse dimensions of the GNRS.

In the second part of this work, we carried out a thermo-plasmonic study of gold nanosphere and gold nanorods in oxygenated human blood. The calculation of the enhanced local electric field at plasmonic resonance gives the possibility to determining the converted heat quantity by these GNPs. Our results show that, at the SPR the local field is strongly enhanced in the vicinity of the nanoparticles, this enhancement is quantified using the exaltation factor, this last depends on the particle shape and does not depend on the intensity of the incident field. Gold nanoparticles at low concentrations deliver remarkable thermal power and heat resistively under a local field exalted at the SPR due to the high resistivity of the smaller nanostructures. In particular we have shown that the local temperature increase in the vicinity of the particle can reach 102 °C and 72 °C respectively for SGNP and GNR during the time 100*s* and for an incident field equal to 10 V/m. After the heat transfer processes in the blood tissue which will homogenize the temperature of the medium, the temperature changes in the medium are calculated depending on the concentration of nanoparticles in ppm units. The increasing temperature of gold nanoparticles depends on a combination of factors, including their geometry and optical absorption efficiency. Our comparison studies with SGNPs, HGNPs, SiO_2/Au, Fe_3O_4/Au and GNRs indicate that all of these gold nanoparticles could absorb and convert NIR light into heat in the blood tissue. By quantifying the amount of heat produced by gold nanoparticles as a function of size and concentration, this study establishes the critical design metrics needed for the formulation of plasmonic nanoparticles to improve non-invasive thermal destruction of cancer.

Authors' contributions AA: Conceptualization, Methodology, Software, Investigation, Validation, Formal analysis, Formal analysis, No funding acquisition, Writing–Original draft preparation, Writing- Reviewing and Editing, Supervision, Project administration. RM: Conceptualization, Methodology, Software, Investigation, Validation, Formal analysis, Formal analysis, No funding acquisition, Writing- Original draft preparation, Writing–Reviewing and Editing, Supervision, Project administration. MB: Conceptualization, Methodology, Software, Investigation, Validation, Formal analysis, Formal analysis, No funding acquisition, Writing- Original draft preparation, Writing–Reviewing and Editing, Supervision, Project administration. AD: Conceptualization, Methodology, Software, Investigation, Validation, Formal analysis, Formal analysis, No funding acquisition, Writing–Original draft preparation, Writing–Reviewing and Editing, Supervision, Project administration.

Funding No funding source.

Availability of data and materials Not applicable.

Declarations Ethical Approval

Not applicable.

Competing interests No competing interests.

References

Akouibaa, A., Masrour, R., Jabar, A., Benhamou, M., Derouiche, A.: Study of optical properties of gold nanoparticles embedded in normal, benign, and malignant breast tissues. J. Mole. Struct. **1244**, 130979 (2021). https://doi.org/10.1016/j.molstruc.2021.130979

Akouibaa, A., et al.: Numerical investigation of electronic, dielectric and optical properties of CdO, SnO2/CdO and SnO2/CdO/PVP nanocomposites. Opt. qua. Elec. **53**, 681 (2021). https://doi.org/10.1007/s11082-021-03305-z

Alison, J.M., Sheppard, R.J.: Dielectric properties of human blood at microwave frequencies. Phys. Med. Biol. **38**(7), 971–978 (1993). https://doi.org/10.1088/0031-9155/38/7/007

Amina, S.J., Guo, B.: A review on the synthesis and functionalization of gold nanoparticles as a drug delivery vehicle. Int. J. Nanomedicine **15**, 9823–9857 (2020). https://doi.org/10.2147/IJN.S279094

Ansal, K.A., Jose, D.S., Rajan, R.K.: Review on biological effect of electromagnetic radiation. In: International Conference on Circuits and Systems in Digital Enterprise Technology, Kottayam, India (2018). https://doi.org/10.1109/ICCSDET.2018.8821217

Baffou, G.: Thermoplasmonics Heating Metal Nanoparticles Using Light. Cambridge University Press. (2017). http://dx.doi.org/https://doi.org/10.1017/9781108289801

Baffou, G., Quidant, R.: Thermoplasmonics: using metallic nanostructures as nanosources of heat. Laser Photon. Rev. **7**(2), 171–187 (2013). https://doi.org/10.1002/lpor.201200003

Bosschaart, N., Edelman, G.-J., Aalders, M.-C.-G., et al.: A literature review and novel theoretical approach on the optical properties of whole blood. Laser Med. Sci. **29**, 453–479 (2014). https://doi.org/10.1007/s10103-013-1446-7

Choi, W.-I., Sahu, A., Kim, Y.-H., Tae, G.: Photothermal cancer therapy and imaging based on gold nanorods. Ann. Biomed. Eng. **40**, 534–546 (2012). https://doi.org/10.1007/s10439-011-0388-0

Crut, A., Maioli, P., Fatti, N.D., Vallée, F.: Optical absorption and scattering spectroscopies of single nano-objects. Chem. Soc. Rev. **43**, 3921–3956 (2014). https://doi.org/10.1039/C3CS60367A

El-Kady, M., El-Sayed, S.M., Fathy, H.E.: development of Galerkin method for solving the generalized Burger's-Huxley equation. Math. Probl. Eng. (2013). https://doi.org/10.1155/2013/165492

Faber, D.-J., van Leeuwen, T.-G.: Are quantitative attenuation measurements of blood by optical coherence tomography feasible. Opt. Lett. **34**, 1435–1437 (2009). https://doi.org/10.1364/OL.34.001435

Faber, D.-J., Aalders, M.-C.-G., Mik, E.-G., Hooper, B.-A.: Oxygen saturation-dependent absorption and scattering of blood. Phys. Rev. Lett. **93**(2), 028102 (2004). https://doi.org/10.1103/PhysRevLett.93.028102

Friebel, M., Meinke, M.: Determination of the complex refractive index of highly concentrated hemoglobin solutions using transmittance and reflectance measurements. J. Biomed. Opt. **10**, 064019 (2005). https://doi.org/10.1117/1.2138027

Friebel, M., Meinke, M.: Model function to calculate the refractive index of native hemoglobin in the wavelength range of 250–1100 nm dependent on concentration. Appl. Opt. **45**, 2838–2842 (2006). https://doi.org/10.1364/AO.45.002838

Gabriel, C., Gabriel, S., Corthout, E.: The dielectric properties of biological tissues: I. Literature survey. Phys. Med. Biol. **41**(11), 2231–2249 (1996a). https://doi.org/10.1088/0031-9155/41/11/001

Gabriel, S., Gabriel, C., Lau, R.-W.: The dielectric properties of biological tissues: II. Measurements in the frequency range 10 Hz to 20 GHz. Phys. Med. Biol. **41**(11), 2251–2269 (1996b). https://doi.org/10.1088/0031-9155/41/11/002

Gabriel, S., Gabriel, C., Lau, R.-W.: The dielectric properties of biological tissues: III. Parametric models for the dielectric spectrum of tissues. Phys. Med. Biol. **41**(11), 2271–2293 (1996c). https://doi.org/10.1088/0031-9155/41/11/003

Ghosh, N., et al.: Simultaneous determination of size and refractive index of red blood cells by light scattering measurements. Appl. Phys. Lett. **88**(8), 084101 (2006). https://doi.org/10.1063/1.2176854

Hu, Y., Fleming, R.C., Drezek, R.A.: Optical properties of gold-silica-gold multilayer nanoshells. Opt. Express **16**(24), 19579–19591 (2008). https://doi.org/10.1364/OE.16.019579

Hu, X., Zhang, Y., Ding, T., Liu, J., Zhao, H.: Multifunctional gold nanoparticles: a novel nanomaterial for various medical applications and biological activities. Front. Bioeng. Biotechnol. **8**, 990 (2020). https://doi.org/10.3389/fbioe.2020.00990

Huang, X., El-Sayed, M.-A.: Gold nanoparticles: optical properties and implementations in cancer diagnosis and photothermal therapy. J. Adv. Res. **1**, 13–28 (2010). https://doi.org/10.1016/j.jare.2010.02.002

Jacques, S.L.: Optical properties of biological tissues: a review. Phys. Med. Biol. **58**(11), R37–R61 (2013). https://doi.org/10.1088/0031-9155/58/11/R37

Jain, P.K., El-Sayed, I.H., El-Sayed, M.A.: Au nanoparticles target cancer. Nano Today **2**(1), 18–29 (2007). https://doi.org/10.1016/S1748-0132(07)70016-6

Kalber, A.T.L., et al.: Hyperthermia treatment of tumors by mesenchymal stem cell-delivered superparamagnetic iron oxide nanoparticles. Int. J. Nanomed. **11**, 1973–1983 (2016). https://doi.org/10.2147/IJN.S94255

Kaur, P., Aliru, M.L., Chadha, A.S., Asea, A., Krishnan, S.: Hyperthermia using nanoparticles: promises and pitfalls. Int. J. Hyperthermia **32**, 76–88 (2016). https://doi.org/10.3109/02656736.2015.1120889

Kumar, S., Mongia, A., Gulati, S., Singh, P., Diwan, A., Shukla, S.: Emerging theranostic gold nanostructures to combat cancer: novel probes for combinatorial immunotherapy and photothermal therapy. Cancer Treat. Res. Com. **25**, 100258 (2020). https://doi.org/10.1016/j.ctarc.2020.100258

Lazebnik, M., McCartney, L., Popovic, D., Watkins, C.-B., Lindstrom, M.-J., Harter, J., et al.: A large-scale study of the ultrawideband microwave dielectric properties of normal breast tissue obtained from reduction surgeries. Phys. Med. Biol. **52**(10), 2637–2656 (2007a). https://doi.org/10.1088/0031-9155/52/10/001

Lazebnik, M., Popovic, D., McCartney, L., Watkins, C.-B., Lindstrom, M.-J., Harter, J., et al.: A large-scale study of the ultrawideband microwave dielectric properties of normal, benign and malignant breast tissues obtained from cancer surgeries. Phys. Med. Biol. **52**(20), 6093–6115 (2007b). https://doi.org/10.1088/0031-9155/52/20/002

Liao, J., Ji, L., Zhang, J., et al.: Influence of the substrate to the LSP coupling wavelength and strength. Nanoscale Res. Lett. **13**, 280 (2018). https://doi.org/10.1186/s11671-018-2691-2

Link, S., Burda, C., Wang, Z.-L., El-Sayed, M.-A.: Electron dynamics in gold and gold-silver nanoparticles: the influence of a non-equilibrium electron distribution and the size dependence of the electron-phonon relaxation. J. Chem. Phys. **111**, 1255–1264 (1999). https://doi.org/10.1063/1.479310

Liu, Q.-J., Zhang, N.-C., Liu, F.-S., Liu, Z.-T.: Structural, electronic, optical, elastic properties and Born effective charges of monoclinic HfO2 from first-principles calculations. Chin. Phys. B **23**(4), 047101 (2014). https://doi.org/10.1088/1674-1056/23/4/047101

Liu, S., Deng, Z., Li, J., Wang, J., Huang, N., Cui, R., Zhang, Q., et al.: Measurement of the refractive index of whole blood and its components for a continuous spectral region. J. Biomed. Opt. **24**(3), 1–5 (2019). https://doi.org/10.1117/1.jbo.24.3.035003

Loghman-Nia, Z., Naderi, M.: Synthesis and characterization of hollow gold nanoparticles by recovery of gold from secondary resources. J. Iran Chem. Soc. **15**, 537–546 (2018). https://doi.org/10.1007/s13738-017-1254-2

Lucarni, V., Saarinen, J.-J., Peiponen, K.-E., Vartiainen, E.-M.: Kramers-Kronig relations in optical materials research. Springer Series in Optical Sciences, (2005). https://www.springer.com/gp/book/9783540236733

Malitson, I.H.: Interspecimen comparison of the refractive index of fused silica. J. Opt. Soc. Am. **55**, 1205–1208 (1965). https://doi.org/10.1364/JOSA.55.001205

Maxwell-Garnett, J.C.: Colours in metal glasses and in metallic films. Philos. Trans. r. Soc. A **203**, 385–420 (1904). https://doi.org/10.1098/rsta.1904.0024

Meinke, M., Muller, G., Helfmann, J., Friebel, M.: Empirical model functions to calculate hematocrit-dependent optical properties of human blood. Appl. Opt. **46**, 1742–1753 (2007). https://doi.org/10.1364/AO.46.001742

Murphy, C.-J., Sau, T.-K., Gole, A.-M., Orendorff, C.-J., et al.: Anisotropic metal nanoparticles: synthesis, assembly and optical applications. J. Phys. Chem. B **109**(29), 13857–13870 (2005). https://doi.org/10.1021/jp0516846

Myroshnychenko, V., Brosseau, C.: Finite-element modeling method for the prediction of the complex effective permittivity of two-phase random statistically isotropic heterostructures. J. Appl. Phys (2005a). https://doi.org/10.1063/1.1835544
Myroshnychenko, V., Brosseau, C.: Finite-element method for calculation of the effective permittivity of random inhomogeneous media. Phys. Rev. E **71**, 016701 (2005b). https://doi.org/10.1103/PhysRevE.71.016701
Nikoobakht, B., El-Sayed, M.-A.: Preparation and growth mechanism of gold nanorods (NRs) using seed-mediated growth method. Chem. Mater. **15**(10), 1957–1962 (2003). https://doi.org/10.1021/cm020732l
Pethig, R.: Dielectric properties of biological materials: biophysical and medical applications. IEEE Trans. Electr. Insul. **5**, 453–474 (1984). https://doi.org/10.1109/TEI.1984.298769
Querry, M.R.: Optical Constants, Missouri Univ-Kansas City, (1985). https://apps.dtic.mil/dtic/tr/fulltext/u2/a158623.pdf
Rashidi-Huyeh, M., Palpant, B.: Counterintuitive thermo-optical response of metal-dielectric nanocomposite materials as a result of local electromagnetic field enhancement. Phys. Rev. B **74**, 75405 (2006). https://doi.org/10.1103/PhysRevB.74.075405
Reddy, J.N.: An Introduction to Finite Element Method, McGraw-Hill Inc. 1993; O.C. Zienkiewicz and R.L. Taylor, The Finite Element Method, Vol. 1, McGraw-Hill, London, 1989.
Sareni, B., Krähenbühl, L., Beroual, A., Brosseau, C.: Effective dielectric constant of periodic composite materials. J. Appl. Phys. **80**(3), 1688–1696 (1996). https://doi.org/10.1063/1.362969
Sienkiewicz, Z.: Biological effects of electromagnetic fields and radiation. In: Ninth international conference on electromagnetic compatibility, conference Publ. No. 396, Manchester, UK, pp. 17–21 (1994). https://doi.org/10.1049/cp:19940670
Sihvola, A.H., Kong, J.A.: Effective permittivity of dielectric mixtures. IEEE Trans. Geosci. Remote Sens. **26**, 420–429 (1988). https://doi.org/10.1109/36.3045
Smith, R.C., Silva, S.R.P.: Interpretation of the field enhancement factor for electron emission from carbon nanotubes. J. Appl. Phys. **106**, 014314 (2009). https://doi.org/10.1063/1.3149803
Steinke, J.-M., Shepherd, A.-P.: Diffuse model of the optical absorbance of whole blood. J. Opt. Soc. Am. A **5**, 813–822 (1988). https://doi.org/10.1364/JOSAA.5.000813
Tan, C.Z.: Determination of refractive index of silica glass for infrared wavelengths by IR spectroscopy. J. Non-Cryst. Solids **223**, 158–163 (1998). https://doi.org/10.1016/S0022-3093(97)00438-9
Tuchin, V.-V.: Handbook of optical biomedical diagnostics. SPIE-The International Society for Optical Engineering, 2nd edn. Bellingham, Washington, 2016. http://lccn.loc.gov/2015038341.
Vial, A., Laroche, T.: Comparison of gold and silver dispersion laws suitable for FDTD simulations. Appl. Phys. B **93**, 139–143 (2008). https://doi.org/10.1007/s00340-008-3202-4
Wasfi, A.S., Humud, H.R., Fadhil, N.K.: Synthesis of core-shell Fe3O4-Au nanoparticles by electrical exploding wire technique combined with laser pulse shooting. Opt. Laser Technol. **111**, 720–726 (2019). https://doi.org/10.1016/j.optlastec.2018.09.006
Wijlemans, J.-W., Bartels, L.-W., Deckers, R., Ries, M., Mali, W.-P., Moonen, C.-T., van den Bosch, M.A.A.J.: Magnetic resonance-guided high-intensity focused ultrasound (MR-HIFU) ablation of liver tumours. Cancer Imaging **12**, 387–394 (2012). https://doi.org/10.1102/1470-7330.2012.9038
Wiley, B.-J., Wang, Z., Wei, J., Yin, Y., Cobden, D.H., Xia, Y.: Synthesis and electrical characterization of silver nanobeams. Nano. Lett. **6**, 2273–2278 (2006). https://doi.org/10.1021/nl061705n
Young, J.-L.: Propagation in linear dispersive media: finite difference time-domain methodologies. IEEE Trans. Antennas Propag. **43**(4), 422–426 (1995). https://doi.org/10.1109/8.376042
Yu-Chen, W., Éric, R., Frédéric, L., Ashok, K.: Synthetic methodologies to gold nanoshells: an overview. Molecules **23**(11), 2851 (2018). https://doi.org/10.3390/molecules23112851
Zhernovaya, O., Sydoruk, O., Tuchin, V., Douplik, A.: The refractive index of human hemoglobin in the visible range. Phys Med Biol. **56**, 4013–4021 (2011). https://doi.org/10.1088/0031-9155/56/13/017